

## Willis Coupling-Induced Acoustic Radiation Force and Torque Reversal

Shahrokh Sepehriahnama<sup>1,\*</sup>, Sebastian Oberst<sup>1,†</sup>, Yan Kei Chiang<sup>2,‡</sup> and David A. Powell<sup>2</sup><sup>1</sup>Centre for Audio, Acoustics and Vibration, University of Technology Sydney, Sydney, NSW 2007, Australia<sup>2</sup>School of Engineering and Information Technology, University of New South Wales, Canberra, ACT 2600, Australia

(Received 4 October 2021; accepted 29 September 2022; published 17 October 2022)

Acoustic meta-atoms serve as the building blocks of metamaterials, with linear properties designed to achieve functions such as beam steering, cloaking, and focusing. They have also been used to shape the characteristics of incident acoustic fields, which led to the manipulation of acoustic radiation force and torque for development of acoustic tweezers with improved spatial resolution. However, acoustic radiation force and torque also depend on the shape of the object, which strongly affects its scattering properties. We show that by designing linear properties of an object using metamaterial concepts, the nonlinear acoustic effects of radiation force and torque can be controlled. Trapped objects are typically small compared with the wavelength, and are described as particles, inducing monopole and dipole scattering. We extend such models to a polarizability tensor including Willis coupling terms, as a measure of asymmetry, capturing the significance of geometrical features. We apply our model to a three-dimensional, subwavelength meta-atom with maximal Willis coupling, demonstrating that the force and the torque can be reversed relative to an equivalent symmetrical particle. By considering shape asymmetry in the acoustic radiation force and torque, Gorkov's fundamental theory of acoustophoresis is thereby extended. Asymmetrical shapes influence the acoustic fields by shifting the stable trapping location, highlighting a potential for tunable, shape-dependent particle sorting.

DOI: 10.1103/PhysRevLett.129.174501

Acoustic radiation force and radiation torque are the physical quantities underlying acoustophoresis—the manipulation of subwavelength objects by an incident acoustic field [1–8]. Applications such as ultrasonic sorting, separation, and levitation have been developed by applying force and torque to objects such as biological cells [7,9–15]. Considering their magnitude relative to gravitational force and fluid drag, acoustic radiation force and torque are most suitable for practical manipulation of subwavelength objects, with sizes ranging from submicrometers to a few millimeters [8,16–24]. Existing theoretical derivations of the acoustic radiation force and radiation torque use simple shapes such as spheres, spheroids, cylinders, and disks, leading to simple expressions which show the influence of the object's volume, material, and aspect ratio [25–31]. An example is the radiation force study of symmetric spherical shells using a phase shift approach that relates the scattering response to physical quantities, such as density and compressibility of a scatterer [32]. This simplifying assumption neglects asymmetry, which is a potential degree of freedom to tune acoustophoretic processes, for example manipulation of a heterogeneous mixture of subwavelength objects, as illustrated in Fig. 1. Neglecting shape asymmetry, Gorkov's theory of acoustophoresis shows that small objects can be trapped at pressure or velocity nodes, cf. Fig. 1(a), depending on their dominant scattering mode [20,33]. However, when shape asymmetry is accounted for, the trapping

locations may shift away from the pressure node, as shown in Fig. 1(b).

Considering the key role of acoustic radiation force and torque in the ultrasonic range, it is important to capture the

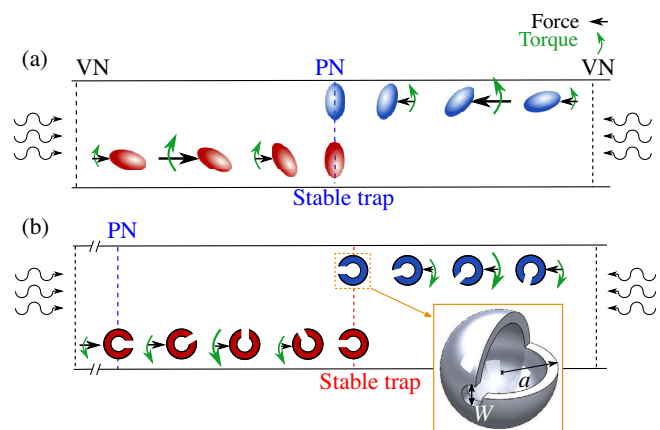


FIG. 1. Acoustic trapping of objects with (a) zero and (b) non-zero Willis coupling, corresponding to symmetric and asymmetric shapes, respectively. The asymmetry in the shape affects the locations of an acoustic trap and the stable orientation of the objects in it. A meta-atom based on a Helmholtz resonator exhibiting such nonconventional acoustic trapping. “PN” and “VN” stand for pressure node and velocity node of an incident acoustic field. “Stable trap” refers to the location of zero radiation force with negative force gradient.

effects of geometric asymmetry on these force and torque fields. Recent advances in asymmetric metamaterials indicate growing interest in designs based on engineered geometries, either as a material of a single meta-atom for beam steering [34–37] or used as a material made of an array of metagratings for beam splitting [38]. Such asymmetric shapes are characterized by Willis coupling, which describes the monopole and dipole moments induced by the incident velocity and pressure fields, respectively [39]. This coupling has a theoretical upper limit and approaches zero as the object approaches a mirror-symmetric configuration [34]. By geometrical modifications such as adding protruding holes and internal cavities, the Willis coupling and its effect on the acoustic field can be controlled [37,39–41]. In particular, a two-dimensional C-shaped Helmholtz resonator can achieve the maximum Willis coupling near its resonance, or other arbitrary values by having multiple apertures of different sizes [36].

To investigate the influence of Willis coupling on the acoustic radiation force and torque, we consider a three-dimensional version of the Helmholtz resonator based meta-atom, as illustrated in Fig. 1(b). The cavity can be considered as a secondary scatterer that is employed to tune the overall scattering response of the meta-atom. Since our design targets the ultrasonic range, narrow and long passages are avoided due to their role in thermoviscous losses [37]. The losses for airborne acoustic meta-materials with narrow passages depend on the depth of the viscous boundary layer, which is inversely proportional to the square root of the frequency and is of the order of micrometers [42]. Here, thermoviscous losses are neglected for the theoretical investigation of shape-controlled meta-material behavior. This assumption is validated in the Supplemental Material [43].

The 3D meta-atom has an internal cavity, occupying 60% of the volume, and one aperture of width  $W = 0.2a$  with  $a$  being the outer radius of the spherical shell, which acts as the normalization parameter, cf. Fig. 1(b). These parameters are tuned to achieve maximum Willis coupling along a single axis [36]. The values of  $a$  are varied from  $0.01\lambda$  to  $0.16\lambda$ , corresponding to  $ka \approx 0.06$  to  $ka \approx 0.96$ , respectively, to investigate the effects of shape asymmetry in the subwavelength range. The monopole-dipole approximation of the scattered pressure field is accurate with less than 5% relative difference, cf. [44–49] for  $ka < 0.2$  and cf. [43] for  $ka < 1$ . Yet, if  $ka > 1$ , higher order terms, e.g., quadrupole, octopole etc., are necessary to obtain a scattered pressure, radiation force, and torque of similar accuracy. We assume that the meta-atom behaves as a sound-hard and immovable object in the acoustic domain. This allows a comparison with existing radiation force theory, which predicts, for a plane standing wave, sound-hard immovable spheres or spheroids are always pushed toward the pressure nodes. These are the stable acoustic trap locations with zero force and negative force gradient,

as illustrated in Fig. 1. For studying radiation torque, a sound-hard immovable prolate spheroid of subwavelength size is used as a reference [50,51]. The radiation force and torque applied to axisymmetric shapes were studied analytically and numerically [48,52]; however, the locations of acoustic traps were the same as in Gorkov’s theory. Here, we demonstrate the correlation between shape asymmetry and the location of an acoustic trap due to the force reversal phenomenon.

The incident field is taken as a plane standing wave with  $p_i = P_a \cos(kz)e^{-j\omega t}$ , and the meta-atom is represented by its monopole-dipole polarizability tensor  $\boldsymbol{\alpha} = \begin{bmatrix} \alpha_{pp} & \alpha_{pv}^T \\ \alpha_{vp} & \alpha_{vv} \end{bmatrix}$ .

The acoustic radiation force and torque are derived as the sum of symmetric and asymmetric terms [53],  $\mathbf{F} = \mathbf{F}_{\text{sym}} + \mathbf{F}_{\text{asym}}$  and  $\mathbf{T} = \mathbf{T}_{\text{sym}} + \mathbf{T}_{\text{asym}}$  with

$$\begin{aligned} \mathbf{F}_{\text{sym}} &= \frac{kE_i}{\rho_f} \left( \frac{\Re[\alpha_{pp}]}{\kappa_f} \mathbf{e}_z - kc_f \Im[\alpha_{vv} \mathbf{e}_z] \cdot \mathbf{e}_z \mathbf{e}_z \right) \sin(2kz), \\ \mathbf{F}_{\text{asym}} &= \frac{kE_i}{\rho_f} c_f \Im[2\alpha_{pv} \cdot (\mathbf{e}_z \mathbf{e}_z)] \cos(2kz), \end{aligned} \quad (1)$$

$$\begin{aligned} \mathbf{T}_{\text{sym}} &= -\frac{kE_i}{\rho_f} c_f \Im[2\alpha_{vv} \mathbf{e}_z] \times \mathbf{e}_z \sin^2(kz), \\ \mathbf{T}_{\text{asym}} &= \frac{kE_i}{\rho_f} \left( \frac{1}{\kappa_f} \Re[\alpha_{vp}] \times \mathbf{e}_z \right) \sin(2kz), \end{aligned} \quad (2)$$

where subscript sym denotes the partial force and torque associated with direct-polarization coefficients  $\alpha_{pp}$  and  $\alpha_{vv}$  [2,53]. The terms with the subscript asym are induced by the Willis coupling coefficients  $\alpha_{pv}$  and  $\alpha_{vp}$ , which obey  $\alpha_{pv} = j\omega\rho_f\alpha_{vp}^T$  for reciprocal media. These terms show the correlation between shape asymmetry and the two fields of acoustic radiation force and torque. This is illustrated in Fig. 1(b), with objects exhibiting strong Willis coupling being trapped in a different location from their symmetric counterparts, cf. Fig. 1(a). Equations (1) and (2) were derived using Gorkov’s far-field approach, from the radiated momentum and the monopole-dipole approximation of the scattered pressure field [53], and are applicable to objects with arbitrary shape in a plane standing wave. Similar expressions for radiation force and torque for other types of incident waves, e.g., Bessel, Gaussian, and vortex beams, can be derived from Eqs. (17) and (24) in Ref. [53]. The polarizability coefficients are calculated numerically using the novel approach in Ref. [53], which is based on the boundary element method and multipole translation and rotation theory. Details of these numerical calculations and the verification study are provided in Ref. [53]. Similar to the torque expression for spheroids, Eq. (21) in Ref. [51],  $T_{\text{sym}}$  in Eq. (2), and Eq. (I.9) in Ref. [43] show the spatial dependences of  $\sin^2(kz)$  and  $\sin(2\theta)$  that apply to objects of arbitrary shape in a plane standing wave.

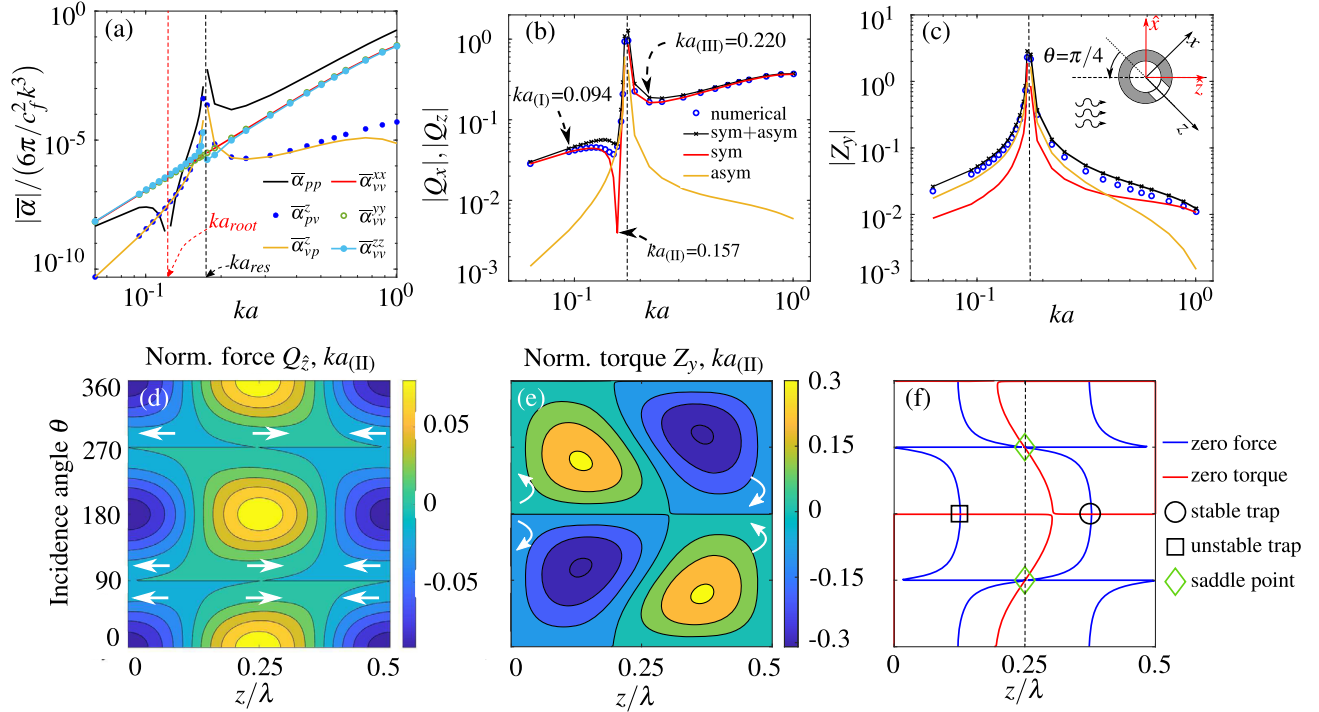


FIG. 2. Panel (a) shows the absolute value of the nonzero and normalized polarizability coefficients  $\alpha$ , for the 3D meta-atom. Normalized radiation force and torque with respect to the size index  $ka$  for the  $\theta = -\pi/4$  incidence angle are shown in panels (b) and (c), respectively. The magnitudes of these quantities are denoted by  $|\mathbf{Q}|$  and  $|\mathbf{Z}|$ . Panels (d) and (e) are the normalized force and torque, respectively, for the case of  $ka_{(\text{II})} = 0.157$  with respect to position  $z/\lambda$  and incidence angle  $\theta$ . The arrows indicate the directions of the force and torque in different regions of panels (d) and (e). Panel (f) shows the loci of zero force and zero torque and locations of saddle points, unstable and stable acoustic traps. Numerical force and torque results are obtained using direct integration of stresses over a fictitious surface enclosing the object.

An incident pressure field of 10 mm wavelength in air is considered, with the speed of sound  $c_f = 343.140 \text{ ms}^{-1}$  and mean density  $\rho_f = 1.204 \text{ kgm}^{-3}$ , to investigate force reversal in airborne levitation within the long wavelength range  $ka < 1$ . The acoustic radiation force and torque values are normalized as force contrast factor  $\mathbf{Q} = \mathbf{F}/(E_i\pi a^2)$  and torque contrast factor  $\mathbf{Z} = \mathbf{T}/(E_i\pi a^3)$ . The energy density of the incident wave is  $E_i = p_i^2/(4\rho_f c_f^2)$ . Although the effects of viscous losses can be captured by the polarizability coefficients, they are neglected since the depth of the viscous boundary layer is at least 3 times smaller than the smallest  $W$  in this study (for validation see the Supplemental Material [43]).

The nonzero coefficients of the normalized polarizability tensor of the meta-atom are shown in Fig. 2(a), with respect to the size index  $ka$ . The results are scaled by  $6\pi/(c_f^2 k^3)$ , which is the maximum permissible value of normalized Willis coupling coefficients [34]. Real and imaginary parts of polarizability coefficients are shown in Fig. (2) of the Supplemental Material [43]. A resonant peak is found at  $ka \approx 0.17$ , and a trough, indicating a zero root, is observed for  $\alpha_{pp}$  at  $ka \approx 0.12$ , implying no contribution from the incident pressure field to the monopole moment. The resonant peak is only observed in the polarizability

coefficients that are associated with the aperture facing the  $z$  direction. These two effects originate from the internal cavity, changing the scattering strength of the monopole mode. The radiation force and torque obtained using Eqs. (1) and (2) are shown with respect to  $ka$  in Figs. 2(b) and 2(c), respectively. The meta-atom is oriented at a fixed angle of  $-\pi/4$  with respect to the positive wave direction  $\hat{z}$ , as shown in the inset of Fig. 2(c), to ensure nonzero torque in the  $y$  direction. The force has two equal components in the  $x$  and  $z$  directions. Equations (1) and (2) are verified by comparing with the force obtained by direct integration of radiation stresses over a fictitious surface of radius  $4\lambda$  enclosing the meta-atom [2,27,53]. The contributions of the direct and Willis-coupling partial forces are plotted in Fig. 2(b). The local minimum in  $Q_{\text{sym}}$  at  $ka \approx 0.157$  emerges due to the root of  $\alpha_{pp}$  at  $ka_{\text{root}} \approx 0.12$ , and  $\alpha_{vv}^{zz}$  being nonzero within this entire range of  $ka$ . The radiation torque exhibits no local minimum since it is independent of the monopole scattering term  $\alpha_{pp}$ , as shown in Eq. (2). The orientation of the object with respect to the wave propagation direction changes the acoustic radiation force and radiation torque, as shown analytically in Ref. [43].

Figures 2(d) and 2(e) show the acoustic radiation force and radiation torque with respect to position  $z$  and

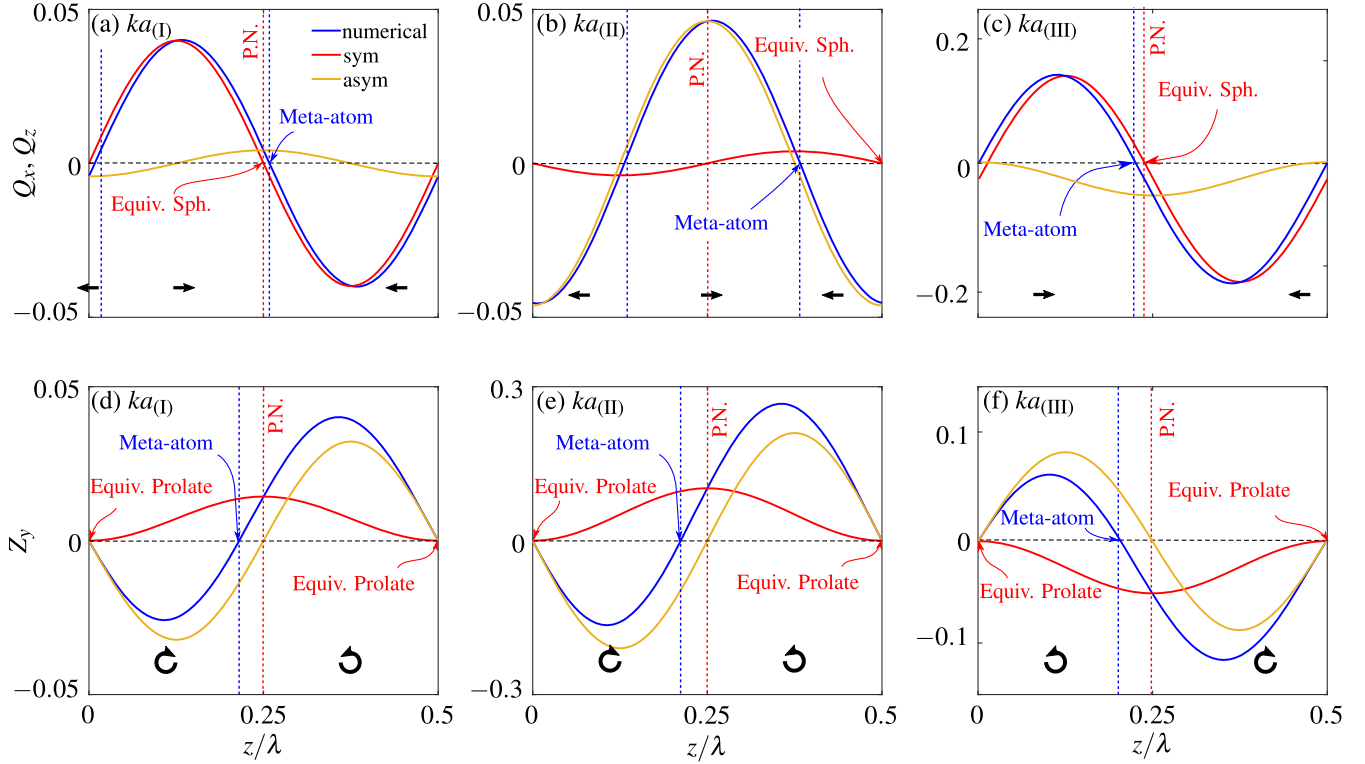


FIG. 3. Variations of the normalized radiation force, panels (a)-(c), and radiation torque, panels (d)-(f), over a half wavelength span between two velocity nodes of a plane standing wave in the  $z$  direction. The results are shown for  $ka_{(I)} = 0.094$  (Rayleigh regime),  $ka_{(II)} = 0.157$  (minimum  $F_{\text{sym}}$ ), and  $ka_{(III)} = 0.220$  (after resonance), and the orientation angle  $\theta = -\pi/4$ . The equivalent spheroid is obtained from the polarizability tensor of the meta-atom by setting the Willis couplings to zero. For the equivalent sphere,  $\alpha_{vv}^{zz}$  is additionally set to  $\alpha_{vv}^{xx}$ . The trap locations of the equivalent sphere and spheroid are found from the analytical expressions in Refs. [2,54] and Refs. [51,55], respectively.

incidence angle  $\theta$  for the specific case of  $ka_{(II)} \approx 0.157$ , at which the radiation force is dominated by the Willis-coupling partial force. The direction of the force and torque are indicated by the arrows in each region. In contrast to the case of symmetric objects, the radiation force is no longer zero at the pressure node  $z/\lambda = 0.25$ , implying a significant shift in the stable trapping location due to shape asymmetry. It is also observed that the force depends on angle  $\theta$ , meaning that the stable acoustic trap occurs where both the force and torque are zero, corresponding to the intersection of the zero contours in Figs. 2(d) and 2(e). These zero force and torque contours are plotted in Fig. 2(f), leading to four intersection points. Only one of these points is stable (circle marker), since both the force and torque gradients are negative. Analysis of the force and torque gradients reveals that the other three points are unstable. For the point marked by a square, any perturbation of position or orientation causes the particle to escape. The points marked with diamonds are saddle points, where particular combinations of torque and force perturbation will lead to the particle escaping.

We now investigate the force and torque distributions at different positions  $z/\lambda$  within the standing wave, as shown

in Fig. 3. A sphere and a prolate spheroid with similar polarizability response to the meta-atom are considered as reference cases, with their acoustic trap being at the pressure node [2,51,53–55]. We quantify the role of Willis coupling as how far the trap location of the meta-atom shifts away from the pressure node. Although equivalent objects are selected based on the polarizability response of the meta-atom, the prediction of their trap location is independent of their size as long as  $ka \ll 1$ . Three different frequency regimes are considered to show the drastic impact of shape asymmetry on the trapping location. Figures 3(a) and 3(d) show the results for  $ka_{(I)} = 0.094$ , corresponding to a low frequency limit where the Willis coupling is much smaller than the direct polarizability terms. As expected, the Willis-coupling partial force [“asym” in Fig. 3(a)] is negligible compared to the direct polarization contribution,  $F_{\text{sym}}$  [“sym” in Fig. 3(a)]. Since  $F_{\text{sym}}$  indicates the net force applied to the equivalent sphere, its trapping point is at the pressure node, where the force is zero with a negative gradient [Fig. 3(a)], matching the results of the classical theory for sound-hard spheres in a plane standing wave [2,16–18,20,33,56]. However, the trap location of the meta-atom determined

by the sum of the two partial forces, shown by the solid blue line, is slightly shifted from the pressure node, as a result of  $F_{\text{asym}}$  being dominant in that region. In Fig. 3(d), we observe the Willis-coupling torque being dominant, resulting in an additional zero-torque location at  $z/\lambda \approx 0.21$ , unlike the reference prolate spheroid that only experiences zero torque at the velocity nodes  $z/\lambda = 0$  and  $z/\lambda = 0.5$  [51,53,55].

In Figs. 3(b) and 3(e), we consider the frequency  $ka_{(\text{II})} = 0.157$ , corresponding to a local minimum of the direct force term  $F_{\text{sym}}$ , so that the total radiation force is determined by the Willis-coupling contribution. This causes the stable trap to shift from the pressure node by  $z/\lambda \approx 0.125$ , to where the symmetric contribution to the force is maximum—illustrating that asymmetric particles can show behavior directly contradicting the conventional Gorkov theory. Although  $F_{\text{sym}}$  is relatively small, we observe a direction reversal of the force vector in comparison to  $ka_{(\text{I})}$ . Such force reversal is typically expected only for  $ka > 1$  [28,57–59], due to the resonant modes of the outer fluid domain. However, our proposed meta-atom undergoes such force reversal due to the internal cavity acting as a Helmholtz resonator and the maximized Willis coupling associated with its single aperture. The net torque is determined by the large contribution from the Willis-coupling partial torque, and the stable angular equilibrium occurs at a point further to the left of the pressure node than for  $ka_{(\text{I})}$ .

After the resonance peak, at  $ka_{(\text{III})} = 0.220$ , the total radiation force and  $F_{\text{sym}}$  shown in Fig. 3(c) exhibit the same direction as predicted by Gorkov theory. We also observe a reversal of the Willis-coupling partial force  $F_{\text{asym}}$ , resulting in a large negative shift of more than  $4a$  from the pressure node. The reversal of the torque shown in Fig. 3(f) indicates its tendency to orient the aperture in the opposite direction to that obtained for  $ka_{(\text{I})}$  and  $ka_{(\text{II})}$ . The stable angular equilibrium is still found at  $z/\lambda \approx 0.21$ , due to the direction reversal of both partial torques. Finally, the relative difference between the results from the monopole-dipole method, cf. Eqs. (1) and (2), and direct force integral method is smaller than 10% at off-resonance frequencies, including the presented cases in Fig. 3. Near the resonant frequency ( $ka \approx 0.169$ ), the monopole-dipole model deviates by up to 40%. Furthermore, the influence of viscosity increases at the near-resonance frequencies [43]. Although adding higher order multipoles, i.e., quadrupole, octopole, and etc., could potentially improve the accuracy of the force and torque estimates at near-resonance frequencies, the direct integral method will provide the theoretical values of these quantities straight away [60].

Our results provide physical insight into the relationship between shape asymmetry and force and torque reversal, which we show here are also possible for  $ka < 1$ . Willis coupling in general describes structure-inherent

asymmetry, which can be related to geometrical anomalies of a trapped object. In addition to anomalous scattering, meta-atoms with strong Willis coupling were shown to experience different acoustic radiation forces and radiation torques, indicating the potential to control these nonlinear acoustic phenomena through Willis coupling. Applications, such as particle sorting, could be tuned to process objects with similar shape features by generating traps at locations other than pressure or velocity nodes. An example is to switch frequency during a sorting process [61], between resonant and off-resonant states, which can be used as a propulsion technique to drive microbots or nanobots between target locations in an acoustofluidic system. Further, single objects can be reoriented, not only in air but also in other fluids, by adjusting the wavelength according to its asymmetric feature size to maximize the Willis coupling. As these effects already take place within the subwavelength regime, target-specific ultrasound manipulation techniques for the control of biological cells, rafts of particles and small tissue ensembles or mesoscopic asymmetrical structures such as insect appendages could be designed by mixing in specifically engineered metaobjects. This control of field quantities using metamaterial concepts for shape-dependent separation of heterogeneous suspension mixtures or adapting self-assembly processes with tailored acoustic beams is likely to provide a fresh approach to the field of acoustophoresis.

This research was supported by the Australian Research Council through Discovery Projects No. DP200101708 and No. DP200100358.

\*shahrokh.sepehrirhanama@uts.edu.au

†sebastian.oberst@uts.edu.au;

Also at School of Engineering and Information Technology, University of New South Wales, Canberra, Australia.

‡Also at Centre for Audio, Acoustics and Vibration, University of Technology Sydney, Sydney, Australia.

- [1] H. Bruus, *Lab Chip* **11**, 3742 (2011).
- [2] H. Bruus, *Lab Chip* **12**, 1014 (2012).
- [3] A. Lenshof, C. Magnusson, and T. Laurell, *Lab Chip* **12**, 1210 (2012).
- [4] H. Bruus, *Lab Chip* **12**, 1578 (2012).
- [5] J. Dual, P. Hahn, I. Leibacher, D. Möller, T. Schwarz, and J. Wang, *Lab Chip* **12**, 4010 (2012).
- [6] M. Wiklund, R. Green, and M. Ohlin, *Lab Chip* **12**, 2438 (2012).
- [7] D. Hartono, Y. Liu, P. L. Tan, X. Y. S. Then, L.-Y. L. Yung, and K.-M. Lim, *Lab Chip* **11**, 4072 (2011).
- [8] A. R. Mohapatra, S. Sepehrirhanama, and K.-M. Lim, *Phys. Rev. E* **97**, 053105 (2018).
- [9] P. Augustsson, C. Magnusson, M. Nordin, H. Lilja, and T. Laurell, *Anal. Chem.* **84**, 7954 (2012).
- [10] A. Bernassau, P. Glynne-Jones, F. Gesellchen, M. Riehle, M. Hill, and D. Cumming, *Ultrasonics* **54**, 268 (2014).

- [11] M. Antfolk, C. Magnusson, P. Augustsson, H. Lilja, and T. Laurell, *Anal. Chem.* **87**, 9322 (2015).
- [12] A. Marzo, S. A. Seah, B. W. Drinkwater, D. R. Sahoo, B. Long, and S. Subramanian, *Nat. Commun.* **6**, 8661 (2015).
- [13] F. B. Wijaya, A. R. Mohapatra, S. Sepehrirahnama, and K.-M. Lim, *Microfluid. Nanofluid.* **20**, 69 (2016).
- [14] A. Marzo and B. W. Drinkwater, *Proc. Natl. Acad. Sci. U.S.A.* **116**, 84 (2019).
- [15] S. Polychronopoulos and G. Memoli, *Sci. Rep.* **10**, 4254 (2020).
- [16] L. V. King, *Proc. R. Soc. A* **147**, 212 (1934).
- [17] K. Yosioka and Y. Kawasima, *Acta Acust. United Acust.* **5**, 167 (1955).
- [18] L. P. Gorkov, *Sov. Phys.-Dokl.* **6**, 773 (1962).
- [19] A. A. Doinikov, *J. Fluid Mech.* **267**, 1 (1994).
- [20] M. Settnes and H. Bruus, *Phys. Rev. E* **85**, 016327 (2012).
- [21] G. T. Silva and H. Bruus, *Phys. Rev. E* **90**, 063007 (2014).
- [22] P. L. Marston, *J. Acoust. Soc. Am.* **120**, 3518 (2006).
- [23] F. Mitri, *Wave Motion* **57**, 231 (2015).
- [24] A. Garcia-Sabaté, A. Castro, M. Hoyos, and R. González-Cinca, *J. Acoust. Soc. Am.* **135**, 1056 (2014).
- [25] A. A. Doinikov, *Proc. R. Soc. A* **447**, 447 (1994).
- [26] D. Foresti, M. Nabavi, and D. Poulikakos, *J. Fluid Mech.* **709**, 581 (2012).
- [27] F. B. Wijaya and K.-M. Lim, *Acta Acust. United Acust.* **101**, 531 (2015).
- [28] F. Mitri, *J. Appl. Phys.* **118**, 214903 (2015).
- [29] W. Wei, D. B. Thiessen, and P. L. Marston, *J. Acoust. Soc. Am.* **116**, 201 (2004).
- [30] W. J. Xie and B. Wei, *Phys. Rev. E* **70**, 046611 (2004).
- [31] A. Garbin, I. Leibacher, P. Hahn, H. Le Ferrand, A. Studart, and J. Dual, *J. Acoust. Soc. Am.* **138**, 2759 (2015).
- [32] X.-D. Fan and L. Zhang, *J. Acoust. Soc. Am.* **150**, 102 (2021).
- [33] S. Sepehrirahnama and K.-M. Lim, *Phys. Rev. E* **102**, 043307 (2020).
- [34] L. Quan, Y. Ra'di, D. L. Sounas, and A. Alù, *Phys. Rev. Lett.* **120**, 254301 (2018).
- [35] J. Jordaán, S. Punzet, A. Melnikov, A. Sanches, S. Oberst, S. Marburg, and D. A. Powell, *Appl. Phys. Lett.* **113**, 224102 (2018).
- [36] A. Melnikov, Y. K. Chiang, L. Quan, S. Oberst, A. Alù, S. Marburg, and D. Powell, *Nat. Commun.* **10**, 3148 (2019).
- [37] Y. K. Chiang, S. Oberst, A. Melnikov, L. Quan, S. Marburg, A. Alù, and D. A. Powell, *Phys. Rev. Appl.* **13**, 064067 (2020).
- [38] H. Ni, X. Fang, Z. Hou, Y. Li, and B. Assouar, *Phys. Rev. B* **100**, 104104 (2019).
- [39] C. F. Sieck, A. Alù, and M. R. Haberman, *Phys. Rev. B* **96**, 104303 (2017).
- [40] X. Su and A. N. Norris, *Phys. Rev. B* **98**, 174305 (2018).
- [41] A. Melnikov, M. Maeder, N. Friedrich, Y. Pozhanka, A. Wollmann, M. Scheffler, S. Oberst, D. Powell, and S. Marburg, *J. Acoust. Soc. Am.* **147**, 1491 (2020).
- [42] X. Jiang, Y. Li, and L. Zhang, *J. Acoust. Soc. Am.* **141**, EL363 (2017).
- [43] See Supplemental Material at <http://link.aps.org/supplemental/10.1103/PhysRevLett.129.174501> for analytical derivation of the force and torque in terms of orientation angle, details of numerical modelling of polarizability coefficients, accuracy of monopole-dipole approximation, and study of the effects of viscous losses (2022).
- [44] S. Sepehrirahnama, K.-M. Lim, and F. S. Chau, *Phys. Procedia* **70**, 80 (2015).
- [45] S. Sepehrirahnama, K.-M. Lim, and F. S. Chau, *J. Acoust. Soc. Am.* **137**, 2614 (2015).
- [46] L. Zhang and P. L. Marston, *J. Acoust. Soc. Am.* **140**, EL178 (2016).
- [47] P. L. Marston, *J. Acoust. Soc. Am.* **142**, 3358 (2017).
- [48] P. L. Marston and L. Zhang, *J. Acoust. Soc. Am.* **141**, 3042 (2017).
- [49] P. L. Marston, *J. Acoust. Soc. Am.* **146**, EL145 (2019).
- [50] J. P. Leao-Neto, M. Hoyos, J.-L. Aider, and G. T. Silva, *J. Acoust. Soc. Am.* **149**, 285 (2021).
- [51] J. P. Leão-Neto, J. H. Lopes, and G. T. Silva, *J. Acoust. Soc. Am.* **147**, 2177 (2020).
- [52] E. B. Lima and T. S. Glauber, *J. Acoust. Soc. Am.* **150**, 376 (2021).
- [53] S. Sepehrirahnama, S. Oberst, Y. K. Chiang, and D. Powell, *Phys. Rev. E* **104**, 065003 (2021).
- [54] P. L. Marston, W. Wei, and D. B. Thiessen, *AIP Conf. Proc.* **838**, 495 (2006).
- [55] Z. Fan, D. Mei, K. Yang, and Z. Chen, *J. Acoust. Soc. Am.* **124**, 2727 (2008).
- [56] S. Sepehrirahnama and K.-M. Lim, *Microfluid. Nanofluid.* **24**, 92 (2020).
- [57] F. Mitri, *Ultrasonics* **49**, 794 (2009).
- [58] L. Zhang, *Phys. Rev. Appl.* **10**, 034039 (2018).
- [59] X.-D. Fan and L. Zhang, *J. Acoust. Soc. Am.* **150**, 102 (2021).
- [60] S. Sepehrirahnama, A. R. Mohapatra, S. Oberst, Y. K. Chiang, D. A. Powell, and K.-M. Lim, *Lab Chip* **22**, 3290 (2022).
- [61] Y. Liu and K.-M. Lim, *Lab Chip* **11**, 3167 (2011).